Available online at www.sciencedirect.com
SCIENCE DIRECT
Journal of Power Sources 155 (2006) 456–460
JOURNAL OF POWER SOURCES
www.elsevier.com/locate/jpowsour

Effect of the Sm content on the structure and electrochemical properties of $La_{1.3-x}Sm_xCaMg_{0.7}Ni_9$ ($x = 0$–0.3) hydrogen storage alloys

Rui Tang [a,b,*], Xuedong Wei [a], Yongning Liu [a], Changchun Zhu [b], Jiewu Zhu [a], Guang Yu [a]

[a] *State Key Laboratory for Mechanical Behavior of Materials, Xi'an Jiaotong University, Xi'an, 710049, China*
[b] *School of Electronic and Information Engineering, Xi'an Jiaotong University, Xi'an, 710049, China*

Received 25 March 2005; received in revised form 7 April 2005; accepted 7 April 2005
Available online 22 June 2005

Abstract

$La_{1.3-x}Sm_xCaMg_{0.7}Ni_9$ ($x = 0$–0.3) hydrogen storage alloys were prepared by inductive melting and the effect of the Sm content on the structure and electrochemical properties was investigated in the paper. The Sm substitution for La in $La_{1.3-x}Sm_xCaMg_{0.7}Ni_9$ ($x = 0$–0.3) alloys does not change the main phase structure (the rhombohedral $PuNi_3$-type structure), but leads to a shrinkage of unit cell and a decrease of hydrogen storage capacity. With the increase of the Sm content in the alloys, the maximum discharge capacity of electrode decreases from 400.2 ($x = 0$) to 346.6 mAh g^{-1} ($x = 0.3$), but the high-rate dischargeability and cycling stability is improved. After 100 cycles, the capacity retention rate increases from 75 ($x = 0$) to 85% ($x = 0.3$).

Keywords: Hydrogen storage alloy; Ni–MH battery; Crystal structure; Electrochemical property

1. Introduction

The nickel–metal hydride (Ni–MH) secondary batteries using AB_5-type hydrogen storage alloys as the negative electrode materials have many advantages, such as high energy density, high dischargeability, long cycle life and environmental compatibility [1]. However, due to the limited capacity (300–320 mAh g^{-1}) of AB_5-type alloys, the energy density of the Ni–MH batteries is not competing with some other advanced secondary batteries.

Recently, a new type of R–Mg–Ni (R = rare earth, Ca, Y) system alloys with $PuNi_3$-type structure have attracted much attention, due to their higher discharge capacity than that of the AB_5-type alloys [2–12]. For example, Chen et al. [6] reported that the discharge capacity of $LaCaMgNi_9$ alloy reached 356 mAh g^{-1}, and almost the same time, Kohno et al. [7] reported that the discharge capacity of $La_{0.7}Mg_{0.3}Ni_{2.8}Co_{0.5}$ alloy reached 410 mAh g^{-1}. However, at present, the R–Mg–Ni system alloys cannot be used as negative material of Ni–MH batteries due to their poor cycling stability. At present, this problem is ameliorated by partial Ce substitution for La and Co, Al substitution for Ni [13–17]. In this paper, it is expected that a proper amount of Sm substitution for La in $La_{1.3}CaMg_{0.7}Ni_9$ alloy may lead to an alloy with high discharge capacity and good cycling stability. The effect of the Sm content on the structure and electrochemical properties of $La_{1.3-x}Sm_xCaMg_{0.7}Ni_9$ ($x = 0$–0.3) hydrogen storage alloys was investigated.

2. Experimental

$La_{1.3-x}Sm_xCaMg_{0.7}Ni_9$ ($x = 0$–0.3) alloys (where all the elements have a purity more than 99.9 wt.%.) were prepared by induction melting under argon atmosphere. To obtain an accurate composition, a little excess of Ca and Mg was considered during preparation because Ca and Mg have high

* Corresponding author. Tel.: +86 29 82669071; fax: +86 29 82669071.
E-mail address: xajttr@163.com (R. Tang).

0378-7753/$ – see front matter © 2005 Elsevier B.V. All rights reserved.
doi:10.1016/j.jpowsour.2005.04.020

vapor pressure and are easy to evaporate. The composition of the prepared alloy ingots was examined by means of atomic absorption spectrometry. The results showed that the difference between the obtained composition and the nominal value was less than 0.01 wt.% for each element. The prepared alloy ingots were mechanically pulverized and the average particle size measured using a JL-9200 laser particle size analyzer is 28 μm.

Crystallographic characterization of the alloys was carried out using a D/max-3A X-ray diffractometer (XRD) with Cu Kα radiation.

The pressure-concentration-temperature (*P–C–T*) curves of the alloys were measured using a Sieverts' type apparatus. At first, the reaction container, which contained 10 g of alloy powder was heated to 353 K and the air was evacuated. After the samples were fully activated through 3 absorbing/desorbing hydrogen cycles, the measurements started.

A amount of 0.5 g of alloy powder mixed well with additive and binding polymer solution was pasted into a porous nickel foam (size 4 cm × 3 cm) and then dried under vacuum at 363 K and finally pressed into the MH working electrode. A $Ni(OH)_2$ electrode (whose preparation process was the same as the working electrode) with a capacity of four times that of the working electrode and a Hg/HgO (6 M KOH) electrode were used as the counter electrode and reference electrode, respectively. The electrochemical properties of the alloy electrodes were measured in a half-cell with 6 M KOH solution at 298 K. The electrode activation and measurements of maximum discharge capacity were carried out at the charge/discharge current of 100 mA g^{-1} with 4 h for charge and the cut-off potential of −0.7 V (versus Hg/HgO) for discharge. The measurements for cycling stability were carried out at the charge/discharge current of 300 mA g^{-1}. To evaluate the dischargeability, the discharge current densities were changed from 100 to 1200 mA g^{-1}. The linear polarization curves of the alloy electrodes were measured at the rate of 0.1 mV s^{-1} from −5 to 5 mV (versus open circuit potential) at 50% depth of discharge (DOD). The hydrogen diffusivity in the bulk of the alloys was evaluated using the potential-step method. After the test electrodes had been fully activated, they lay up in fully charged state until their potential reached the equilibrium potential, and then an overpotential of +200 mV was applied to these electrodes. The current–time transient curves were recorded after the potential step. The measurements of linear polarization and potential step were conducted using a PS-168 electrochemical interface analyzer.

3. Results and discussion

3.1. Crystal structure

Fig. 1 shows the XRD patterns of $La_{1.3-x}Sm_xCaMg_{0.7}Ni_9$ (x = 0–0.3) alloys. It is found that all the alloys contain a main phase with the rhombohedral $PuNi_3$-type structure and a very few minor impurity phase including $LaNi_5$ and $LaNi_2$. The crystallographic parameters are listed in Table 1. It can be seen that the Sm substitution for La in the alloys leads to a decrease of lattice constants and a shrinkage of unit cell due to the atomic radius of Sm (1.80 Å) being smaller than that of La (1.88 Å). Besides, the value of *c*/*a* shows a small increase, indicating that the increase of Sm content in the alloys leads a less decrease of the *c*-axis than that of the *a*-axis. The unit cell volume of as a function of x in $La_{1.3-x}Sm_xCaMg_{0.7}Ni_9$ is shown in Fig. 2. It is found that

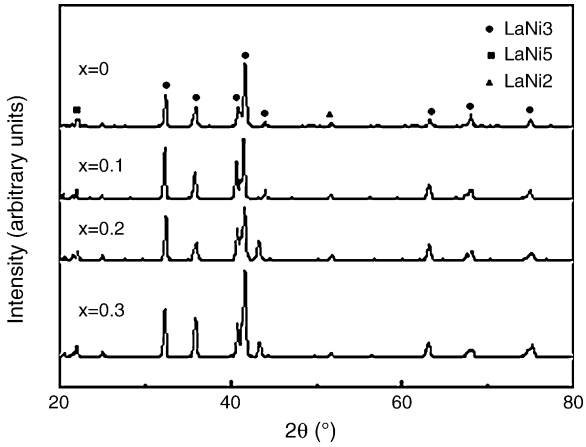

Fig. 1. XRD patterns of $La_{1.3-x}Sm_xCaMg_{0.7}Ni_9$ (x = 0–0.3) alloys.

Table 1
Crystallographic data of $La_{1.3-x}Sm_xCaMg_{0.7}Ni_9$ (x = 0–0.3) alloys

Samples (x)	Lattice constants			Unit cell volume (Å^3)
	a (Å)	c (Å)	c/a	
0	5.013	23.030	4.595	501.2
0.1	5.005	23.028	4.601	499.6
0.2	4.996	23.024	4.608	497.7
0.3	4.988	23.013	4.614	495.9

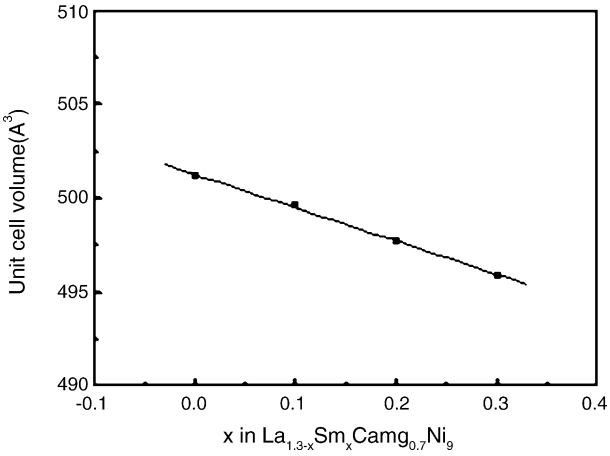

Fig. 2. Variation of the unit cell volume as a function of x in $La_{1.3-x}Sm_xCaMg_{0.7}Ni_9$ (x = 0–0.3) alloys.

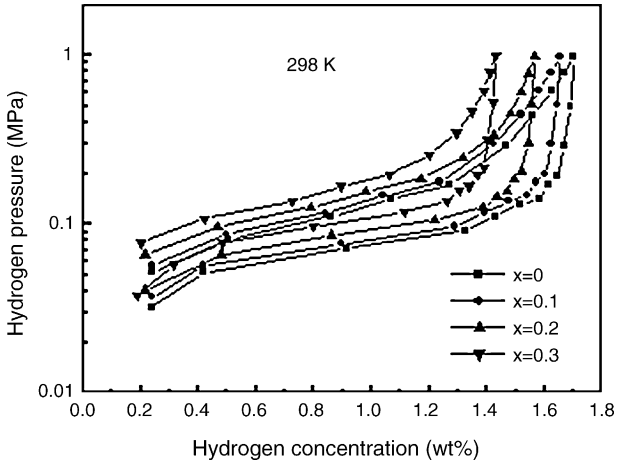

Fig. 3. *P–C–T* curves of $La_{1.3-x}Sm_xCaMg_{0.7}Ni_9$ ($x=0$–0.3) alloys for hydrogen absorption and desorption.

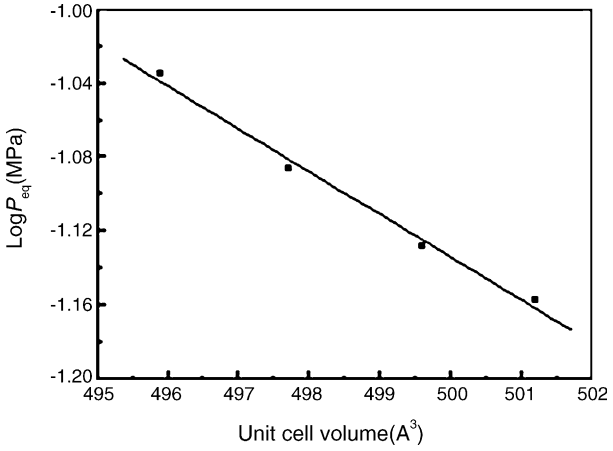

Fig. 4. Variation of the desorption plateau pressure as a function of the unit cell volume of $La_{1.3-x}Sm_xCaMg_{0.7}Ni_9$ ($x=0$–0.3) alloys.

the cell volume is a linear function of the Sm content. The cell volume is of interest because it can be corrected with the stability of hydride phase in any homologous alloy series [18].

3.2. Thermodynamic characteristics

Fig. 3 shows the *P–C–T* curves of $La_{1.3-x}Sm_x$ $CaMg_{0.7}Ni_9$ ($x=0$–0.3) alloys at 298 K. It can be seen that with the increase of the Sm content in the alloys, the plateau region becomes narrower, which leads to the decrease of hydrogen storage capacity from 1.7 ($x=0$) to 1.43 wt.% ($x=0.3$). The variation of the *P–C–T* curve characteristics can be attributed to the reduction of the unit cell volume. It is generally accepted that hydrogen storage alloys with larger unit cell volumes would result in more sites available for hydrogen storage. Besides, the plateau pressure for hydrogen absorption and desorption increases noticeably as the Sm content in the alloys increases. This result indicates that the stability of hydride reduces with increasing Sm content of the alloy. Fig. 4 shows the relationship between the unit cell volumes of the alloys and the plateau pressures for hydrogen desorption at 298 K. A linear correlation between $\log P_{eq}$ and the unit cell volume is observed, which is similar to most AB_5-type alloys [19].

3.3. Electrochemical properties

The activation properties and maximum discharge capacity of $La_{1.3-x}Sm_xCaMg_{0.7}Ni_9$ ($x=0$–0.3) alloy electrodes at the discharge current density of 100 mAh g^{-1} are listed in Table 2. It can be seen that these alloys can be activated to reach their maximum capacity within five cycles. With the increase of the Sm content in the alloys, the maximum discharge capacity decreases from 400.2 ($x=0$) to 346.6 mAh g^{-1} ($x=0.3$). The variation of maximum discharge capacity is in agreement with the variation of the hydrogen storage capacity measured. Besides, it is also found that the utilization efficiency of alloy increases from 88.6 ($x=0$) to 91.3% ($x=0.3$) as the increase of Sm content results in less stability of hydride and better electrochemical kinetics. As a results, the maximum discharge capacity of the $La_{1.3-x}Sm_xCaMg_{0.7}Ni_9$ alloys with $x=0$–0.2 is noticeably higher than that of the commercialized AB_5-type alloys.

The dischargeability of $La_{1.3-x}Sm_xCaMg_{0.7}Ni_9$ ($x=0$–0.3) alloy electrodes, expressed as the percentage of C_d to C_{100} (where C_d and C_{100} are the discharge capacity at the discharge current density of I_d and 100 mA g^{-1}, respectively), is shown in Fig. 5, It is found that the Sm substitution for La in the alloys resulted in a better high-rate dischargeability (HRD). It can be seen from Table 2 that the increase of the Sm content in the alloys, the HRD increases from 38.2 ($x=0$) to 53.4% ($x=0.3$) at the discharge current density of 1200 mAh^{-1}. In electrochemical cells, the HRD of metal hydride electrode is determined by the charge transfer process at the metal/electrolyte interface and the mass transfer (hydrogen diffusion) process in the bulk of alloy particles [20]. These electrochemical characteristics were investigated as follows.

The electrocatalytic activity of metal hydride surface during the charge transfer reaction is evaluated using surface

Table 2
Electrochemical properties of $La_{1.3-x}Sm_xCaMg_{0.7}Ni_9$ ($x=0$–0.3) alloy electrodes

Samples (x)	C_{max} (mAh g^{-1})	N_a[a]	HRD_{1200}[b] (%)	S_{100} (%)
0	400.2	2	38.2	75
0.1	389.5	3	42.5	77
0.2	373.8	3	46.7	81
0.3	346.6	5	53.4	85

[a] The cycle numbers needed to activate the electrodes.
[b] The high-rate dischargeability at the discharge current density of 1200 mA g^{-1}.

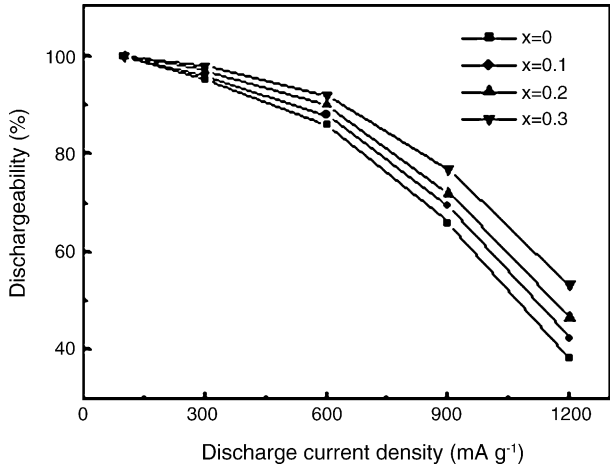

Fig. 5. Dischargeability of $La_{1.3-x}Sm_xCaMg_{0.7}Ni_9$ (x = 0–0.3) alloy electrodes.

activation enthalpy (ΔH^*), which can be calculated from the temperature dependence of the charge transfer resistance (R_d) according to the following equation [21]

$$\ln(T/R_d) = C_0 - \Delta H^*/RT \quad (1)$$

where T is the absolute temperature, C_0 is a constant including surface area, R is the gas constant. The R_d value can be calculated from the slope of linear polarization curve according to the following equation [22]

$$R_d = \eta/I \quad (2)$$

where η is the total overpotential, I is the applied current. Fig. 6 shows the plots of $\ln(T/R_d)$ versus $1/T$. It was found that all the plots exhibited good linear relations. The ΔH^* values are listed in Table 3. It can be seen that with the increase of the Sm content in the alloys, the ΔH^* value decreases. This result indicates that the electrocatalytic activity of hydride increases with increasing Sm content in the alloys.

Table 3
Surface activation enthalpy and hydrogen diffusion coefficients of $La_{1.3-x}Sm_xCaMg_{0.7}Ni_9$ (x = 0–0.3) alloy electrodes

Sample (x)	ΔH^* (KJ mol^{-1})	D ($\times 10^{-10}$ m^2 s^{-1})
0	27.33	3.86
0.1	25.97	5.14
0.2	24.28	7.69
0.3	21.87	8.80

Fig. 7 shows the semilogarithmic curves of anodic current–time responses of $La_{1.3-x}Sm_xCaMg_{0.7}Ni_9$ (x = 0–0.3) alloy electrodes. The diffusion coefficient of hydrogen in the bulk of the alloys can be calculated through the linear portion of the responding plots in Fig. 7 according to the following equation [20]

$$\log i = \log(6FD/da^2)(C_0 - C_s) - (\pi^2 D/2.303a^2)t \quad (3)$$

where i, D, d, a, C_0, C_s and t are the diffusion current (A g^{-1}), the diffusion coefficient of hydrogen (cm^2 s^{-1}), the density of the hydrogen storage alloy (g cm^{-3}), the alloy particle radius (cm), the initial hydrogen concentration in the bulk of the alloy (mol cm^{-3}), the hydrogen concentration on the surface of the alloy particles (mol cm^{-3}) and the discharge time (s), respectively. Using the average particle radius (a = 28 μm), the D values are calculated and also listed in Table 3. It can be seen that with the increase of the Sm content in the alloys, the D value increases, indicating that the hydrogen diffusivity within the bulk of the alloy particles accelerates. This result can be ascribed to the reduction of the stability of hydrides due to the decrease of the unit cell volume.

Fig. 8 shows the cycling stability of $La_{1.3-x}Sm_xCaMg_{0.7}Ni_9$ (x = 0–0.3) alloy electrodes. The cycling

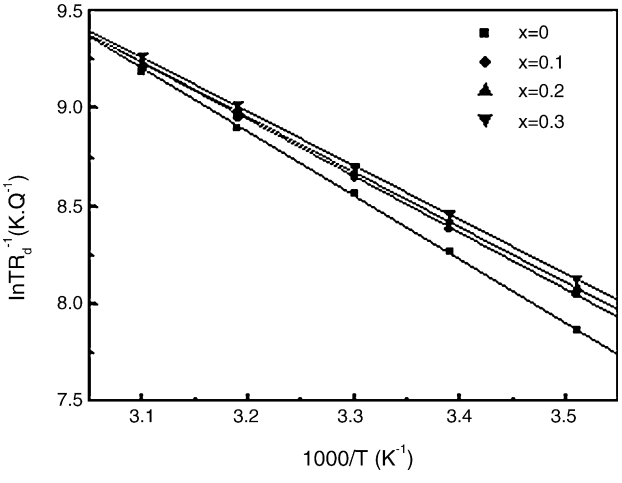

Fig. 6. Plots of $\ln(T/R_d)$ vs. $1/T$ of $La_{1.3-x}Sm_xCaMg_{0.7}Ni_9$ (x = 0–0.3) alloy electrodes.

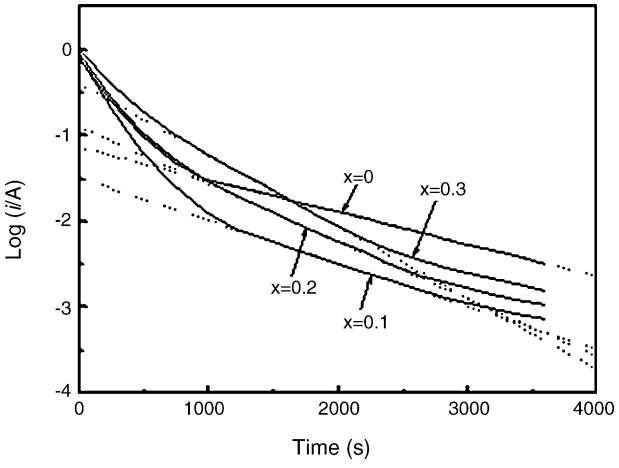

Fig. 7. Semilogarithmic plots of anodic current–time responses of $La_{1.3-x}Sm_xCaMg_{0.7}Ni_9$ (x = 0–0.3) alloy electrodes after the potential step (+200 mV).

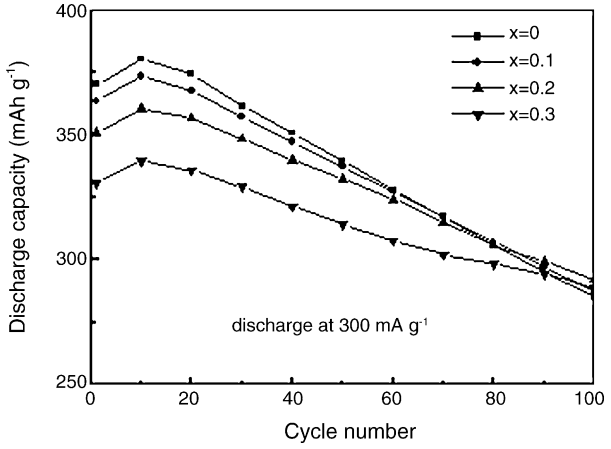

Fig. 8. Cycling stability of $La_{1.3-x}Sm_xCaMg_{0.7}Ni_9$ ($x=0$–0.3) alloy electrodes.

capacity retention rate, also listed in Table 2, is expressed as

$$S_{100} = C_{100}/C_{max} \times 100\% \quad (4)$$

where C_{100} is the maximum discharge capacity, C_{max} is the discharge capacity at the 100th cycle. It can be seen that with the increase of the Sm content in the alloys, the capacity retention rate increases from 75 ($x=0$) to 85% ($x=0.3$). This result can be ascribed to the decrease of the unit cell volume with increasing Sm content. It is generally believed that the volume change of an alloy during hydriding is proportional to the amount of hydrogen absorbed in cycling. The increase of Sm leads to a lower hydrogen storage and smaller change of unit cell volume on hydriding and hence less pulverization and improvement in the cycling stability.

4. Conclusions

The Sm substitution for La in $La_{1.3-x}Sm_xCaMg_{0.7}Ni_9$ ($x=0$–0.3) alloys does not change the main phase structure (the rhombohedral $PuNi_3$-type structure), but leads to a shrinkage of unit cell and a decrease of hydrogen storage capacity. With the increase of the Sm content in the alloys, the maximum discharge capacity of electrode decreases from 400.2 ($x=0$) to 346.6 mAh g^{-1} ($x=0.3$), but the high-rate dischargeability and cycling stability is improved. After 100 cycles, the capacity retention rate increases from 75 ($x=0$) to 85% ($x=0.3$).

Acknowledgements

The authors are grateful for the supports of the present work by Education Ministry Key Foundation, Shannxi Industrial Project and Doctoral Foundation.

References

[1] T. Sakai, I. Uehara, H. Iwakura, J. Alloys Compd. 293–395 (1999) 762.
[2] K. Kadir, T. Sakai, I. Uahara, J. Alloys Compd. 257 (1997) 115.
[3] K. Kadir, N. Nuriyama, T. Sakai, I. Uehara, L. Eriksson, J. Alloys Compd. 284 (1999) 145.
[4] K. Kadir, T. Sakai, I. Uahara, J. Alloys Compd. 287 (1999) 264.
[5] J. Chen, H.T. Takeshita, H. Tanaka, N. Kuriyama, T. Sakai, J. Alloys Compd. 302 (2000) 304.
[6] J. Chen, N. Kuriyama, H.T. Takeshita, H. Tanaka, T. Sakai, M. Haruta, Electrochem. Solid-State Lett. 3 (2000) 249.
[7] T. Kohno, H. Yoshida, F. Kawashima, T. Inaba, I. Sakai, M. Yamamoto, M. Kanda, J. Alloys Compd. 311 (2000) L5.
[8] R. Tang, L.Q. Liu, Y.L. Liu, G. Yu, Int. J. Hydrogen Energy 28 (2003) 815.
[9] H.G. Pan, Y.F. Liu, M.X. Gao, Y.F. Zhu, Y.Q. Lei, Int. J. Hydrogen Energy 28 (2003) 1219.
[10] H.G. Pan, Y.F. Liu, M.X. Gao, Y.Q. Lei, Q.D. Wang, J. Alloys Compd. 351 (2003) 228.
[11] B. Liao, Y.Q. Lei, G.L. Lu, X.L. Chen, H.G. Pan, Q.D. Wang, J. Alloys Compd. 356–357 (2003) 746.
[12] H.G. Pan, Y.F. Liu, M.X. Gao, Y.Q. Lei, Q.D. Wang, J. Electrochem. Soc. 150 (2003) A565.
[13] H.G. Pan, Q.W. Jin, M.X. Gao, Y.F. Liu, R. Li, Y.Q. Lei, J. Alloys Compd. 373 (2004) 237.
[14] Y.F. Liu, H.G. Pan, M.X. Gao, R. Li, Y.Q. Lei, J. Alloys Compd. 376 (2004) 296.
[15] Y.F. Liu, H.G. Pan, M.X. Gao, R. Li, Y.Q. Lei, J. Alloys Compd. 376 (2004) 304.
[16] B. Liao, Y.Q. Lei, X.L. Chen, G.L. Lu, H.G. Pan, Q.D. Wang, Electrochem. Acta 50 (2004) 1057.
[17] H.G. Pan, Y.F. Liu, M.X. Gao, Y.Q. Lei, Q.D. Wang, J. Electrochem. Soc. 152 (2005) A326.
[18] D.N. Gruen, M.H. Mendelsohn, A.E. Dwight, J. Less-Common Met. 19 (1977) 56.
[19] J.J. Reilly, Metal hydrides electrodes, in: J.O. Besenhard (Ed.), Handbook of Battery Materials, Wiley, New York, 2000.
[20] G. Zhang, B.N. Popo, R.E. Whit, J. Electrochem. Soc. 142 (1995) 2695.
[21] N. Kuriyama, T. Saka, H. Miyamur, I.H. Uehida, Ishikawa, J. Alloys. Compd. 192 (1993) 161.
[22] P.H.L. Notten, P. Hokkeling, J. Electrochem. Soc. 138 (1991) 1877.